THE ASTROPHYSICAL JOURNAL, 305:684–697, 1986 June 15

HIGH DYNAMIC RANGE VLBI OBSERVATIONS OF NGC 6251

DAYTON L. JONES,[1] S. C. UNWIN, A. C. S. READHEAD, W. L. W. SARGENT, AND G. A. SEIELSTAD[2]
Owens Valley Radio Observatory, California Institute of Technology

R. S. SIMON
Naval Research Laboratory

R. C. WALKER, J. M. BENSON, R. A. PERLEY, AND A. H. BRIDLE
National Radio Astronomy Observatory

I. I. K. PAULINY-TOTH, J. ROMNEY,[3] AND A. WITZEL
Max-Planck-Institut für Radioastronomie

P. N. WILKINSON
Jodrell Bank

L. B. BÅÅTH AND R. S. BOOTH
Onsala Space Observatory

D. N. FORT
Algonquin Radio Observatory

J. A. GALT
Dominion Radio Astrophysical Observatory

R. L. MUTEL
University of Iowa

AND

R. P. LINFIELD[4]
Hat Creek Radio Observatory
Received 1985 August 2; accepted 1985 December 12

ABSTRACT

The large radio galaxy NGC 6251 has been observed with an 11 telescope VLBI array, including the full VLA, at 18 cm. We present high dynamic range maps of both the VLBI– and VLA–scale radio structure from these observations, as well as hybrid maps from earlier VLBI experiments at 6 and 13 cm. The 18 cm VLBI hybrid map has an unusually high dynamic range of ~300 to 1 (ratio of the peak brightness to five times the rms noise level) and is limited by thermal noise rather than calibration errors. A lower limit of 80 to 1 for the ratio of jet/counterjet brightness at parsec scales can be set. This is the strongest such limit produced by VLBI observations of any source to date. If the absence of a detectable counterjet is caused by relativistic beaming, then the jet must be aligned within 45° of our line of sight. Our VLA map shows a complex structure along the previously detected kiloparsec-scale counterjet. We discuss the physical conditions in the inner few parsecs of the NGC 6251 jet and their relation to the conditions in the extraordinarily long and well collimated kiloparsec-scale jets and show that both small- and large-scale morphology can be explained in terms of a simple model and relativistic beaming.

Subject headings: galaxies: individual — galaxies: jets — galaxies: nuclei — interferometry — radio sources: galaxies

I. INTRODUCTION

It is well known that the large-scale (kpc-Mpc) structure of many extragalactic radio sources is symmetric (e.g., Miley 1980), but that some of the most powerful objects have asymmetric structure. This raises the interesting question, succinctly posed by Wheeler (1971), of "whether there are two distinct mechanisms for producing jets, one symmetric, the other monodirectional or [whether] there is only a symmetric mechanism" since "considerations of timing, Doppler effect and density give much opportunity for a symmetric mechanism to show up unsymmetric in the observations."

A remarkable result has emerged in radio astronomy over the last decade which forces us to add a third possibility to the two considered by Wheeler in 1970. This is the fact that the small-scale (pc) nuclear radio structure is often asymmetric (e.g., Kellermann and Pauliny-Toth 1981) even in objects which are symmetric on the large scale. This raises the possibility of a basic mechanism which is monodirectional but switches from side to side, giving rise to symmetric large-scale radio structure due to the accumulation of matter on both sides of the nucleus over a number of switching cycles. These "flip-flop" models have been considered by many authors (see,

[1] Currently an NRC-NASA Research Associate at the Jet Propulsion Laboratory, California Institute of Technology, Pasadena.
[2] Currently at the National Radio Astronomy Observatory, Green Bank, West Virginia.
[3] Currently at the National Radio Astronomy Observatory, Charlottesville, Virginia.
[4] Currently at the Jet Propulsion Laboratory, California Institute of Technology, Pasadena.

for example, Rudnick 1984; Bridle 1984, and references cited therein). Thus, we now have to consider the possibility of a basically unsymmetric mechanism showing up symmetric in the observations.

In many cases large-scale radio jets are seen which connect the active nucleus with the outer lobes (e.g., Bridle and Perley 1984), and it is found that lower luminosity objects have two-sided jets, while higher luminosity objects have one-sided jets.

There is clearly a connection between the large- and small-scale asymmetries, since in all powerful sources with both large- and small-scale radio jets (19 cases) the small-scale jet is on the same side of the nucleus as the large-scale jet. This rules out explanations of the small-scale asymmetry based on obscuration by matter, since it is inconceivable that the large-scale counterjets are similarly obscured. It also complicates the explanation based on switching, since the large-scale asymmetric jets would also have to switch, and this places a lower limit on the switching time which is hard to reconcile with the statistics and sizes of symmetric objects (Readhead 1980).

The simplest remaining explanation for the observations is the Doppler effect. This is an attractive possibility, as there is now strong evidence, based both on proper motion studies and on combined radio and X-ray observations (see Cohen and Unwin 1984), that the parsec-scale radio emission regions in many asymmetric cores are moving at relativistic speed, and thus that Doppler effects must strongly affect the appearance of these objects. If the small-scale asymmetry is caused by the Doppler effect, then this must also be responsible for the large-scale asymmetry. However, there is clear evidence that the bulk velocity along some large-scale radio jets is not relativistic. In low-luminosity objects (e.g., Burch 1977; Perley, Willis, and Scott 1979), the observed symmetry of the jets makes this obvious. For the high-luminosity objects the case is not nearly so clear, and it is possible that the ubiquitous one-sidedness of the jets seen in these objects is due to Doppler beaming.

The observation of a nuclear counterjet in a symmetric object would show that the basic jet-producing mechanism is two-sided (at least in some objects) and might provide more stringent limits against which the Doppler beaming hypothesis could be tested. We therefore decided to make sensitive VLBI observations of a symmetric object to search for a nuclear counterjet. NGC 6251 was selected for this purpose for the following reasons:

1. It is an object of intermediate luminosity, and therefore if the bulk velocity is correlated with luminosity, the radiation from a counterjet will be less strongly beamed and thus easier to detect than in high-luminosity objects.

2. It has both a jet and a counterjet on large scales. The ratio of brightness of the jet to the counterjet varies from about 30:1 to greater than 300:1 (Perley, Bridle, and Willis 1984). If the brightness ratio in the nucleus is similar, then there is a possibility of detecting the counterjet with VLBI observations.

3. The object is large (1.8 Mpc projected), and therefore the axis of the source is probably within $\sim 60°$ of the plane of the sky (otherwise it would be one of the largest radio sources known). Thus, if Doppler beaming is important, the jet/counterjet brightness ratio will not be as extreme as in the case of an object aligned along our line of sight.

4. The central component of NGC 6251 is fairly bright, so it can be observed with the narrow-band Mark II VLBI system, which is available at a large number of telescopes.

5. The object is at a high declination, so good (u, v) coverage can be obtained and a high-quality hybrid map can be made.

TABLE 1

SYSTEM TEMPERATURES AND TELESCOPE SENSITIVITIES AT 18 cm

TELESCOPE	SYSTEM TEMPERATURE (K)	SYSTEM TEMPERATURE (Jy)	SENSITIVITY (K/Jy)
Onsala 26 m	28	299	0.0935
MPI 100 m	41	28	1.443
WSRT (1 × 25 m)	58	617	0.094
Jodrell 76 m	102	127	0.805[a]
ARO 46 m	220	733	0.30
NRAO 43 m	52	205	0.254
Iowa 18 m	90	1915	0.047
VLA (27 × 25 m)	65	26	2.50
OVRO 40 m	51	237	0.215
Hat Creek 26 m	53	564	0.094
Penticton 26 m	82	901	0.091

[a] Peak.

II. OBSERVATIONS

The observations reported here were performed during a 27.5 hr period on 1983 March 29–30. Fourteen telescopes were scheduled, although two of these did not participate due to equipment failures and the Haystack telescope was withdrawn from the experiment to support a satellite rescue mission. The remaining 11 telescopes are listed in Table 1, along with their measured system temperatures and sensitivities. Figure 1 shows the (u, v) coverage obtained with this array.

The Mk II VLBI recording system (Clark 1973; Moran 1976) was used, providing a 1.8 MHz bandwidth centered on 1660.9 MHz. Left circular polarization was recorded at all stations. Six stations used hydrogen maser frequency standards, while the other five used rubidium standards. The data were correlated on the NRAO three-station processor during the summer of 1983.

The experiment was scheduled as a series of 90 minute observations of NGC 6251 alternating with 30 minute observations of one of the calibration sources listed in Table 2. These calibrators were selected because previous VLBI experiments indicated that they were very compact. The number of 30 minute observations of each calibrator varied from five for 0235+164 to one for DA 193. The use of several calibration sources is necessary if baseline-dependent gain corrections are to be made, since with a single calibrator there is no way to distinguish between the effects of incorrect baseline calibration and those due to source structure.

An exception to the observing schedule described above was required at the VLA, where we used the full phased array. Since the extended emission associated with NGC 6251 prevents real-time phasing of the VLA, it was necessary to observe a nearby point source (1803+784) every 30 minutes. This took only a few minutes and thus did not reduce the observing time

TABLE 2

VLBI CALIBRATION SOURCES

Source	Total Flux Density (Jy)	Number of 30 Minute Scans
0016+731	0.94	2
0235+164	2.05	5
DA 193	1.89	1
OQ 208	0.99	2
1739+522	2.12	3

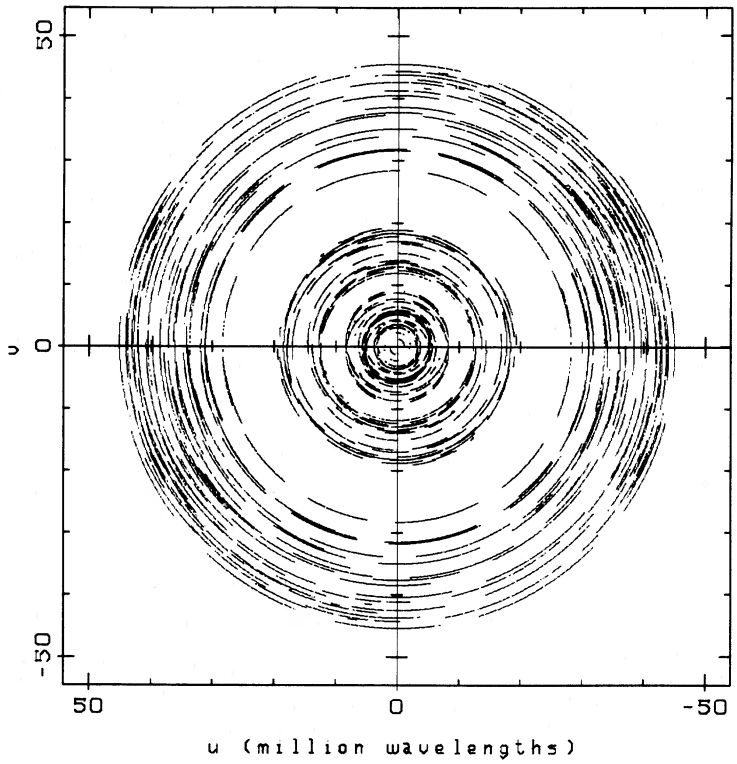

FIG. 1.—The (u, v) coverage of NGC 6251 obtained during the 18 cm VLBI experiment. Each point represents a 60 s integration.

on NGC 6251 significantly. As a result of the phased array observations, we were able to make a very high quality VLA map of the kiloparsec-scale jet in addition to the VLBI map.

III. DATA REDUCTION

This was one of the most extensive VLBI observations undertaken thus far. Our goal was to make a hybrid map with unusually high dynamic range. The procedure used is described in some detail, in order that others can benefit from our experience.

The integration time at the processor was 2 s, which was later averaged to 4 s to reduce the data file to a manageable size. Amplitude and phase corrections were applied to the data before averaging, to correct for machine delay and fractional-bit-shift effects. When the fringe rate was near zero (fewer than 3 cycles per integration period) the fractional-bit-shift correction could not be applied accurately, and these data were deleted. The corrected, averaged data were then Fourier-transformed into four frequency channels (each 0.5 MHz wide) and transferred from the NRAO/SAO VLBI format into AIPS format. The AIPS global fringe-fitting program (Schwab and Cotton 1983), with a point source input model, was used on the data from NGC 6251 and each of the calibrators. It was assumed that a point source model was reasonably accurate for the calibrators but not for NGC 6251. Therefore, the fringe fitting for the calibrators was done using both the FFT and least-squares algorithms and with 1, 2, and 3 baseline combinations (see Schwab and Cotton 1983). For NGC 6251, only an FFT fringe search was done.

The resulting visibilities were coherently averaged for 60 s, and a hybrid map of NGC 6251 was made from this data set. This showed a jet about 15 mas long in position angle 300°. Only amplitude calibration based on measured system temperatures and telescope gains (Cohen *et al.* 1975) was used at this point. The initial map was used as an input model for a second iteration of fringe fitting on the original 4 s visibility data.

For the second iteration, the least-squares solutions using 1, 2, and 3 baseline combinations were calculated. Tests of global fringe fitting with a small subset of the NGC 6251 data showed that the current source model was sufficiently good for all baseline combinations and a narrower search window (± 600 ns in delay, ± 300 mHz in rate) to be used. The resulting data set was much better; it had less scatter in the visibilities and more fringe detections on the weaker baselines than the first set produced by the FFT-only fringe fitting. In both cases, a solution interval of 60 s was used.

One a reasonably good set of fringe solutions had been produced, more care was needed in editing and calibration. The 4 s data points were therefore edited before being coherently averaged to 60 s. This was a tedious process, as there were more than a million visibility amplitudes and phases to inspect. The system temperature and telescope gain calibration was then applied to the edited and averaged data, and additional station gain corrections derived from the calibrators were applied.

The additional gain corrections were determined by making hybrid maps of the calibrators and using three iterations of time-independent amplitude self-calibration (Cornwell and Wilkinson 1981) to improve these maps. The station gain corrections were seen to be similar for all the sources and thus were applied to the NGC 6251 data as well. For some stations, these corrections were large ($\sim 10\%$), indicating that normal VLBI calibration, even when done carefully and at a wavelength where most telescopes are very well behaved, can still be surprisingly inaccurate. Since these gain corrections were

derived from the calibrators, which were unresolved at all telescopes, the station calibrations were not affected by any partially resolved radio emission. We searched for baseline-dependent calibration errors by examining the fit of the hybrid maps to the data for each calibrator. No baselines were found to have systematically high or low amplitudes for most of the calibrators. Our upper limits for baseline-dependent gain errors were less than 5% for the most sensitive baselines and 10%–15% for the less sensitive baselines. Such errors will almost certainly be important when mapping stronger sources (where much higher dynamic ranges should be possible in principle) but are probably not important for relatively weak sources such as NGC 6251.

A third hybrid map was made from this new data set, which showed extended structure out to approximately 28 mas. However, attempts at improving this map with self-calibration were not successful. Furthermore, the noise level on the maps was several times higher than the theoretical noise level. We suspected that data from the least sensitive baselines were causing the problem. On most baselines the signal-to-noise ratio was large enough that it was relatively easy to identify the occasional bad 4 s points prior to averaging. However, on the weaker baselines the signal-to-noise ratio before averaging was too low to permit this. Therefore, the data from these baselines were contaminated by an unknown fraction of spurious data points. This problem did not occur with the calibrators, since they all produced strong fringes.

In an attempt to improve the fringe-fitting results for the weak baselines, a final iteration of global fitting was done. The 4 s output points from the last global fitting iteration, before being averaged in frequency, were used as the input, and the current best map was used as the model. The delay and rate windows were narrowed to ± 250 ns and ± 100 mHz, and the solution interval was reduced to 24 s to allow more accurate correction of atmospheric and ionospheric effects. The shorter solution interval was also selected to avoid coherence problems at some of the weaker stations, which were known to have relatively poor rubidium clocks. Note that a partial loss of coherence will not only reduce sensitivity but will also corrupt the closure relations. A much longer solution interval (several minutes) would have improved the weak baseline sensitivity if loss of coherence were not a problem. It was found that careful editing of the reference antenna (VLA) data prior to fringe-fitting improved the quality of the global fit. This was done by removing all VLA data during times when the phased-array amplitudes were low, indicating that the array was not completely phased up.

The result of this final fringe-fitting iteration was an improvement in the shorter baselines, for which the more extended structure in the input map provided a more accurate model, but only a small improvement in the weakest baselines. The narrower search window reduced the number of erroneous detections, but the baseline phases were still scattered over a large range of angles. It is possible that a much narrower search window could have been used.

We deleted all data from baselines for which the phase scatter was more than $\sim 30°$ peak to peak. This resulted in a significant improvement in the final map. There were 20 such baselines. Ten of these were baselines to Hat Creek, which contained very little data due to technical problems at Hat Creek during the observations. Figure 2 shows the reduced (u, v) coverage caused by the removal of the 20 weakest baselines of the initial 55 baselines.

The removal of the weakest baselines had a large effect because these baselines were given artificially high weight in the mapping process. This occurred because we used uniform

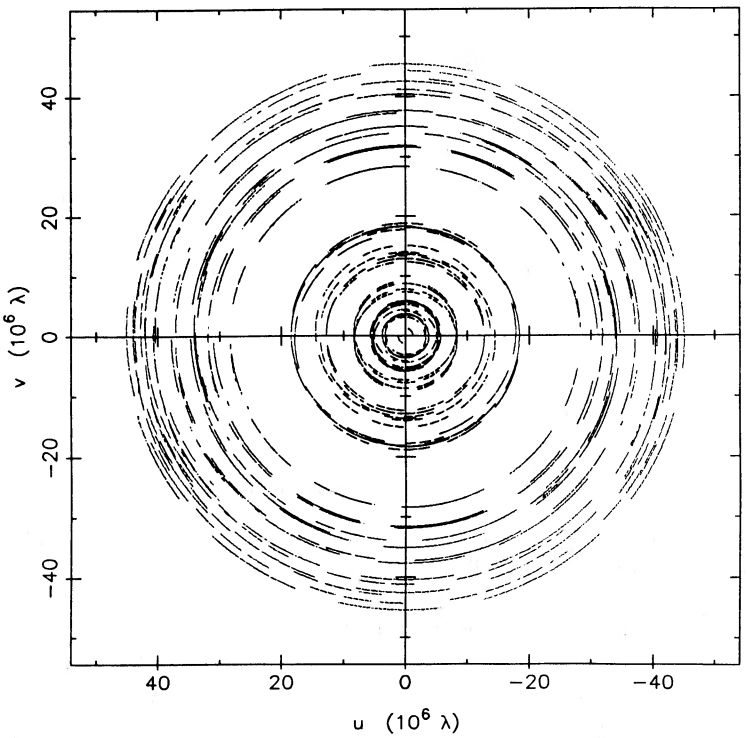

FIG. 2.—The (u, v) coverage of NGC 6251 remaining after all low signal-to-noise baselines have been removed

weighting rather than natural weighting when making the maps (to obtain higher angular resolution), and also because it is not possible to discriminate accurately between good and bad data points in data with a low signal-to-noise ratio. Spurious points contribute only noise, and no signal. This means that the true signal-to-noise ratio for the averaged weak data is smaller than the value determined from the errors on all the data points which were averaged together. In principle it is possible to estimate the number of false detections and hence to correct the weighting. This correction should be incorporated into the standard fringe-fitting procedures.

After editing and calibration as described above, the data were coherently averaged for 60 s and a hybrid map was made using self-calibration in the usual way. Both the Caltech and NRAO AIPS mapping programs were used (independently) and found to produce similar results. A total of five iterations was made, starting with one iteration of phase-only corrections and continuing with amplitude corrections on decreasing time scales. Since the starting model was thought to be a better fit to the longer baselines, the shorter baselines (less than 30×10^6 wavelengths) were given less weight during the first few iterations. The resulting map is shown in Figure 3. We also made a hybrid map from data which had been coherently averaged for 240 s, with essentially identical results.

This analysis required approximately 50 hr of CPU time on a DEC VAX-11/780 computer with FPS AP-120B array processor, but this includes time spent exploring different techniques and correcting occasional mistakes.

IV. RESULTS

a) 18 cm *VLBI Hybrid Map*

Several interesting features are revealed in Figure 3. First, the basic morphology is the familiar one of a one-sided core-jet source. We assume that the brightest peak is the core, as it is unresolved (FWHM < 2 mas). The measured jet/counterjet brightness ratio at ± 6 mas from the core is greater than 80:1. Second, the brightness of the jet declines rapidly during the first 12 mas, then declines more slowly. Third, there is a local brightening of the jet 25 mas (11 pc projected, using a Hubble constant of 75 km s^{-1} Mpc^{-1}) from the core. The peak brightness of this "knot" is just over 1% of the central core. Fourth, the jet appears unresolved perpendicular to its length. This implies that the opening angle (FWHM/distance) of the jet over its first 15–20 mas is less than 7°. Finally, the position angle from the core to the knot is different from the position angle of the inner 15 mas of the jet. This difference is $3^\circ.5 \pm 1^\circ.0$, which accounts for most (but not all) of the misalignment between the parsec- and kiloparsec-scale jet position angles found by Cohen and Readhead (1979). The direction of the jet bending is toward the optical minor axis (Young *et al.* 1979), in agreement with the results of Cohen and Readhead. This bending is discussed in more detail below.

Figure 4 shows the measured noise level in the map of NGC 6251 as a function of radial distance from the central peak. In regions more than ~35 mas from the central peak, the measured rms noise is 0.2 mJy per beam. The theoretical noise level for this array (e.g., Fomalont and Wright 1974), allowing for the unavoidable increase in noise caused by the hybrid mapping process (Cornwell 1981; Wilkinson 1983), is 0.19 mJy per beam. Thus, we have probably reached the highest dynamic range possible for this data, at least in regions far from the core. The ratio of peak brightness to the rms noise level is greater than 1300 to 1. A more useful measure of map quality is the uniqueness of weak features, but this is not easily quantified. It is not yet known whether a similar effort of repeated editing, fringe-fitting, and calibration on data from a strong VLBI source would also result in a thermally noise-limited map. If so, VLBI dynamic ranges of several thousand to one should be possible for the strongest compact sources. It

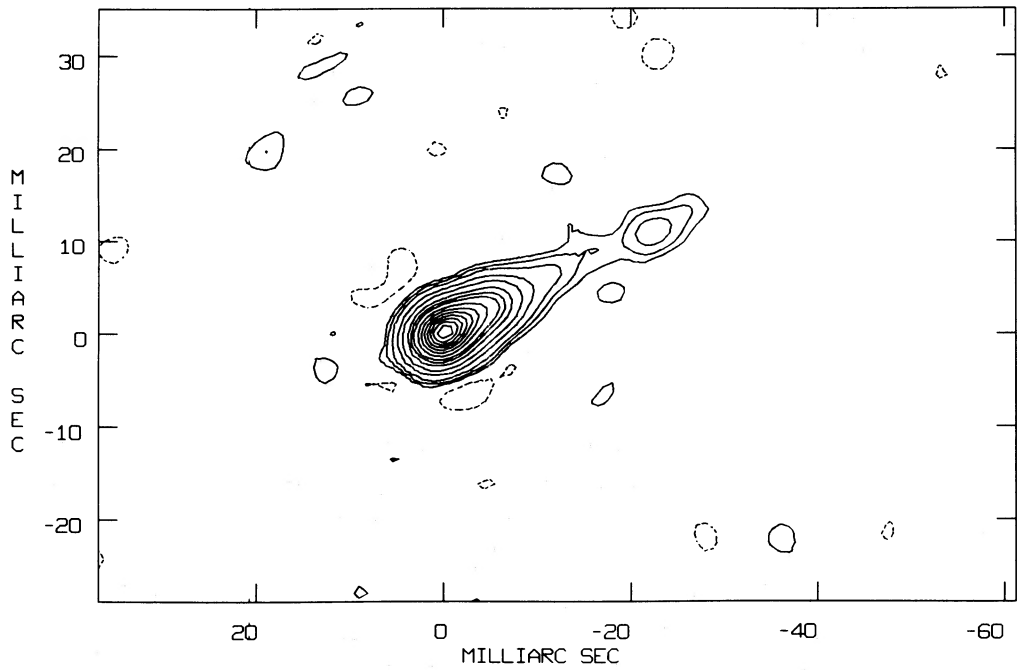

FIG. 3.—A VLBI hybrid map of NGC 6251 at 18 cm. The contours are −0.25, 0.25, 0.5, 1, 2, 5, 10, 15, 25, 35, 50, 70, and 90% of the peak, which equals 279 mJy per beam. The clean beam was circular with FWHM = 3.0 mas.

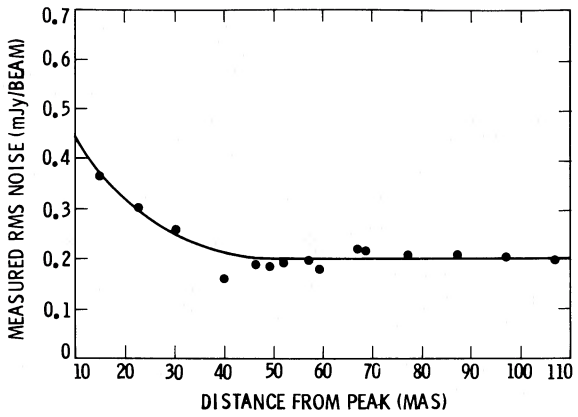

FIG. 4.—Measured rms noise level, in mJy per beam, as a function of distance from the central peak of the map. Each point represents the rms calculated over rectangular regions of either 546 or 1701 pixels. The distances plotted are from the center of the map (peak intensity) to the center of each rectangular region.

is likely that baseline-dependent calibration errors will be the limiting factor in these cases.

An area much larger than that shown in Figure 3 was searched for more extended radio emission. This was done by applying a Gaussian taper to the (u, v) data and convolving the resulting map with a larger beam. No peaks as large as 0.5% of the central peak were found within 250 mas (0.11 kpc projected) of the center, except for the structure shown in Figure 3. The central part of the tapered hybrid map is shown in Figure 5. Note that this map has been rotated clockwise by 30°.0.

b) 6 cm *VLBI Hybrid Map*

In addition to the 18 cm VLBI hybrid map, we have a lower dynamic range 6 cm hybrid map, shown in Figure 6. It was made from data obtained during a five-station Mk II VLBI experiment in 1981 December and shows the jet extending to 7–8 mas. The telescopes used for these observations were the MPI 100 m, Haystack 37 m, NRAO 43 m, Fort Davis 26 m, and OVRO 40 m antennas. The frequency band was 1.8 MHz wide, centered on 4989.1 MHz, and right circular polarization was recorded. The data were correlated on the CIT/JPL five-station processor in Pasadena.

Comparison of the 6 and 18 cm VLBI maps shows that the position angle at 6 cm agrees with that of the inner part of the 18 cm map, as expected. The core is more dominant at 6 cm, implying that it has an inverted spectrum between 6 and 18 cm. This assumes that the peak on each map is in fact the core. The unresolved core flux density is 0.36 Jy at 6 cm and 0.28 Jy at 18 cm, but these are not simultaneous measurements. Note that at 6 cm the brightness of the jet appears to be nearly constant between about 3 and 6 mas from the core, while at 18 cm the jet brightness appears to be decreasing rapidly throughout this region. This may be an artifact of the lower resolution available at 18 cm. It must be remembered that compact radio sources are often variable, and consequently detailed comparisons of maps from different epochs to get spectral information is risky. We can set a lower limit of 5 to 1 for the jet/counterjet brightness ratio at 6 cm.

c) 13 cm *VLBI Hybrid Map*

We have also made a 13 cm hybrid map from data obtained in 1980 February. A different five-station VLBI array was used, consisting of the Jodrell Bank 76 m, Haystack 37 m, OVRO 40 m, and two NASA Deep Space Network 64 m telescopes (Madrid and Goldstone). The 1.8 MHz wide frequency band was centered on 2290.9 MHz, and left circular polarization was used. These data were also correlated on the CIT/JPL processor. Although the same number of stations was used at 6 and 13 cm, the (u, v) coverage at 13 cm was not as good as at 6 cm due to shorter observing time (8 hr instead of 12). The 13 cm VLBI hybrid map is shown in Figure 7. Although this map has a slightly lower dynamic range than the 6 cm map, the jet is stronger at 13 cm, and this allows us to set a lower limit of 6 to 1 for the jet/counterjet brightness ratio.

Three of the telescopes we used at 13 cm were also used for observations of NGC 6251 at the same frequency by Cohen and Readhead (1979). A comparison of data on the common baselines between these experiments, 1.7 yr apart, indicates that there has been some change in structure. In particular, there is evidence for small ($\sim 10\%$) changes in visibility amplitudes on the very sensitive and well-calibrated baseline

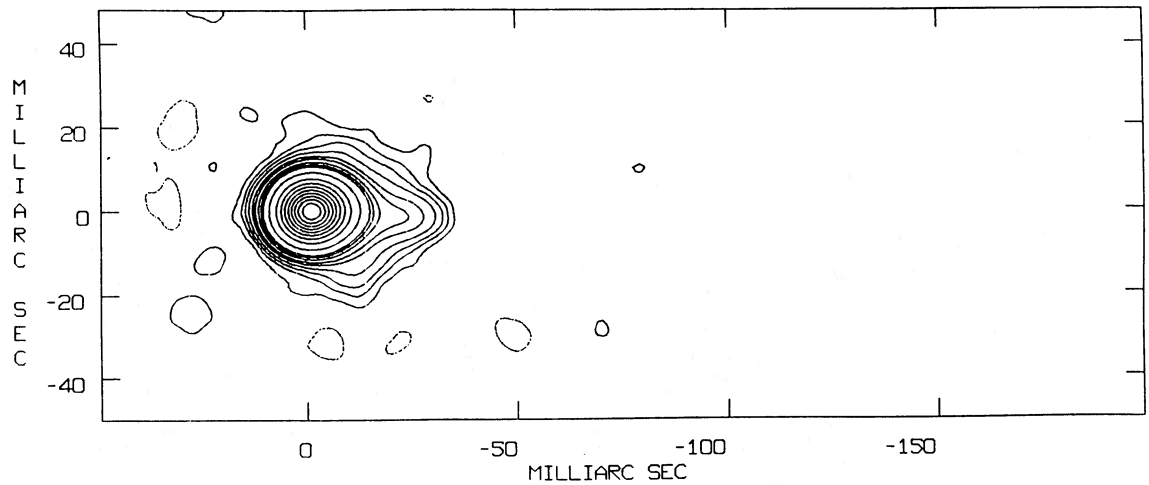

FIG. 5.—A VLBI hybrid map made from tapered (u, v) data and convolved with a larger beam to search for extended, low surface brightness radio emission. The source has been rotated by 30°.0 clockwise in this map. The contours are 0.3, 0.5, 0.7, 1.0, 1.5, 2, 3, 4, 5, 10, 20, 30, 40, 50, 60, 70, 80, and 90% of the peak, which equals 421 mJy per beam. The 50% contour shows the size of the clean beam.

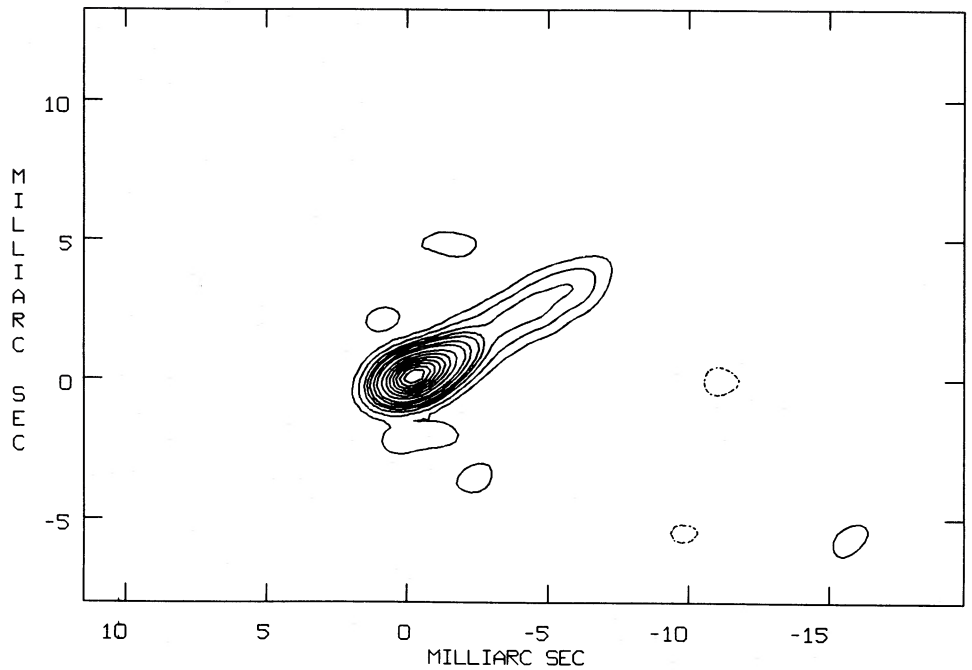

FIG. 6.—A VLBI hybrid map of NGC 6251 at 6 cm. The contours are −1.0, 1.0, 2.5, 5.0, 7.5, 10, 15, 20, 30, 40, 50, 60, 70, 80, and 90% of the peak, which equals 350 mJy per beam. The clean beam was 1.3 × 1.1 mas (FWHM), with the major axis in position angle 90°.

between the NASA Deep Space Network stations at Madrid and Goldstone. This evidence is shown in Figure 8. By model-fitting the two 13 cm epochs, we find that a decrease in the core flux by ∼15% is the simplest explanation for these changes. The one closure phase triangle in common to both epochs (Madrid-Goldstone-OVRO) shows a mean closure phase difference of 1°.3 ± 6°.9, consistent with no significant change in structure. However, this closure phase is dominated by the phase due to source structure on the short Goldstone-OVRO baseline.

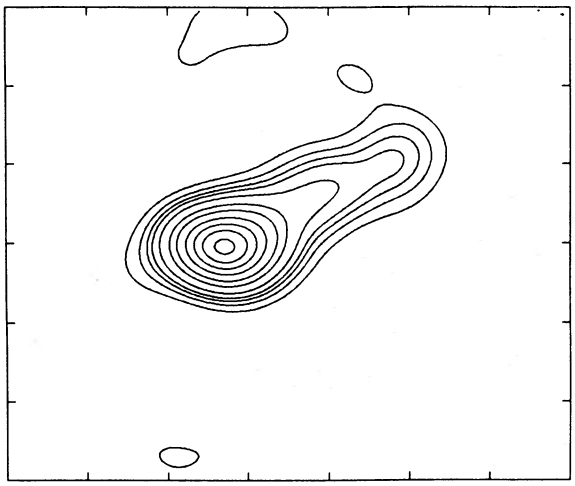

FIG. 7.—A VLBI hybrid map of NGC 6251 at 13 cm. The contours are 2.5, 5.0, 7.5, 10, 15, 25, 35, 50, 65, 80, and 95% of the peak, which equals 247 mJy per beam. The clean beam was 2.5 × 1.8 mas (FWHM), with the major axis in position angle 60°. The tick marks along the axes are 3 mas apart.

d) Curvature of the Inner Jet

The first report of a misalignment between the parsec and kiloparsec radio jets in NGC 6251 was made by Readhead, Cohen, and Blandford (1978). This was confirmed by Cohen and Readhead (1979) with better data. Their published position angle for the parsec-scale jet was for 1978.4, the epoch of observation. When precessed to 1950.0, this position angle is 302°.2 ± 0°.8. The mean position angle of the first 120″ of the kiloparsec-scale jet, also for epoch 1950.0, is 296°.4 ± 0°.1 (Perley, Bridle, and Willis 1984). The difference is 5°.8 ± 0°.8. Our measured (and precessed to 1950.0) position angles for the parcsec-scale jet are 301°.8 ± 1° at 6 cm, 299°.0 ± 3° at 13 cm, and 300°.4 ± 1° for the inner 10 mas at 18 cm. The position angle of the knot 25 mas from the core in the 18 cm hybrid map is 296°.9 ± 1°. This agrees very well with the kpc jet position angle, indicating that nearly all of the jet curvature occurs less than 25 mas from the core.

The VLBI measurements are consistent with a bending of 1°–2° from less than 4 mas to ∼10 mas, a further bending of ∼4° between ∼10 mas and ∼25 mas, and less than 0°.5 of bending at larger distances from the center. A simple model in which the jet position angle decreases by 0°.24 mas^{-1} out to 27 mas from the center and then remains constant fits the existing measurements, although it is unlikely that the true jet curvature is this constant or that it stops so abruptly. Figure 9 shows the measured position angle of the NGC 6251 jet as a function of angular distance from the core.

The apparent curvature of this jet is much less than that seen in many "superluminal" compact radio sources. However, it is believed that the radio jets in "superluminal" sources are oriented nearly along our line of sight. This would cause their intrinsic curvature to appear greatly magnified by projection. Assuming that the jet in NGC 6251 is not oriented within a few degrees of our line of sight, it is possible that the intrinsic

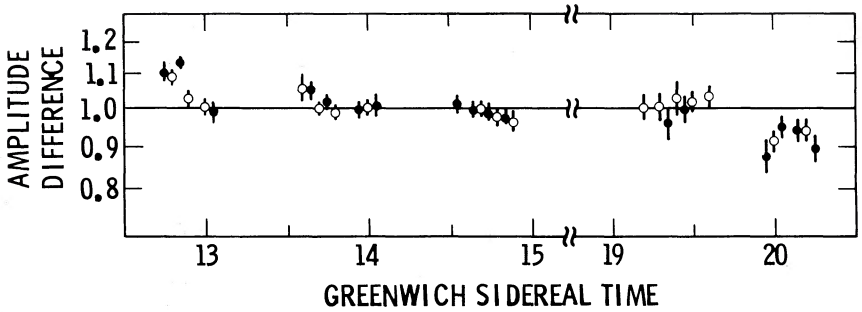

FIG. 8.—Ratio of visibility amplitudes between 1978 May and 1980 February at 13 cm on the Madrid-Goldstone baseline. The amplitudes have been normalized to the mean of all points in common to allow for differences in the absolute flux scales between the epochs. This assures that the mean ratio will be unity. There are data from two separate days in 1978 May corresponding to 1978.35 and 1978.37. *Open circles*, ratio of 1980.09/1978.35 amplitudes; *filled circles*, ratio of 1980.09/1978.37 amplitudes. The error bars show $\pm 1\ \sigma$ random errors only. Pointing errors are thought to be very small ($< 1\%$) at these stations, and variations in the system temperature due to ground pickup will tend to cancel in the ratio.

curvature of its nuclear segment is similar to the intrinsic curvature of radio jets in "superluminal" sources.

e) 18 cm *VLA Phased Array Maps*

The VLA phased array maps from our 18 cm VLBI experiment are shown in Figures 10 and 11. The VLA was in the C configuration during these observations, giving a synthesized beam size (FWHM) of $\sim 10''$. Because of the high declination of NGC 6251 and the long (24 hr) tracking time, the beam is almost perfectly circular and has very low sidelobes. The resulting dynamic range (the ratio of peak brightness to five times the off-source rms noise level) is well over 1000 to 1, with rms noise below 0.1 mJy per beam. Several background sources stronger than 0.5 mJy can be seen in both maps. In both maps, the brightest peak corresponds to the position of the optical nucleus of the galaxy, and the compact radio structure shown in the VLBI maps is located within this central peak.

Figure 10 is a map of the inner parts of the kiloparsec-scale jet and counterjet, showing the counterjet out to more than 4′ from the core. It can be seen that the counterjet is nearly linear out to this distance and has several knots (local brightness maxima) along its length. The brightest of these, 1′ (27 kpc projected) from the core, has a peak brightness of ~ 1.4 mJy per beam. The counterjet fades from this brightest knot toward the core. At 0.′5 from the core, the counterjet brightness is only ~ 0.8 mJy per beam. This is ~ 65 times fainter that the main jet at the same distance from the core.

Figure 11 is a larger field map, showing the complex structure of the "warm" spot in the northwest radio lobe ($\sim 15'$ from the core). Flux densities near the edge of this map are less reliable than near the center, because the single-dish HPBW ($\sim 27'$) is about the same size as the field shown.

We have also made a map of the entire VLA field of view. This map shows the counterjet out to nearly 17′ (460 kpc projected) from the core. This is discussed in detail in § VII.

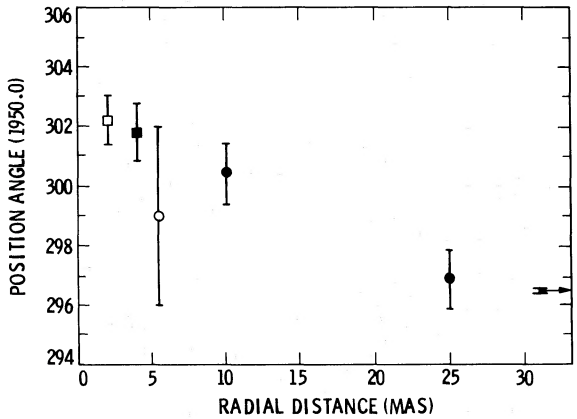

FIG. 9.—Plot of position angles measured by VLBI as a function of distance from the core. All position angles have been precessed to epoch 1950.0. *Filled circles*, from our 18 cm hybrid map; *open circle*, from our 13 cm hybrid map; *filled square*, from our 6 cm hybrid map; *open square*, from Cohen and Readhead (1979). The arrow at the right edge of the plot shows the VLA-measured position angle of the first 120″ of the large-scale jet.

V. PHYSICAL PROPERTIES

Table 3 gives values for various physical parameters which are calculable from our VLBI measurements. We have assumed that each component of the source can be modeled as a uniform sphere (for the core) or cylinder (for the jet) emitting synchrotron radiation. We also assumed that there is no bulk motion of the radio-emitting region other than that due to the cosmological recession of its host galaxy (with a Hubble constant of 75 km s^{-1} Mpc^{-1}). Note that if this assumption is not valid, some of the calculated quantities could be incorrect by orders of magnitude. In particular, the magnetic field energy density would be underestimated and the relativistic electron energy density overestimated if the observed radiation was relativistically beamed in our direction.

Figure 12 shows the radio spectrum of NGC 6251, decomposed into separate spectra for different parts of the source.

TABLE 3

PHYSICAL PARAMETERS FOR PARSEC-SCALE RADIO STRUCTURE IN NGC 6251

Parameter	Core	Jet
Maximum frequency (GHz)	13.50	3.60
Maximum flux density (Jy)	0.67	0.72
Angular diameter (mas)	<0.20	$<0.5 \times 5.0$
Assumed source geometry	Sphere	Cylinder
Optically thin spectral index	-0.25	-0.75
Luminosity (ergs s^{-1})	6×10^{41}	2×10^{41}
Brightness temperature (K)	$>2 \times 10^{11}$	$>3 \times 10^{10}$
Magnetic field (G)	<0.7	<2.0
Radiative lifetime (yr)	>0.5	>0.2
Magnetic energy density (ergs cm^{-3})	<0.02	<0.2
Electron energy density (ergs cm^{-3})	$>9 \times 10^{-4}$	$>6 \times 10^{-7}$
Electron/magnetic energy density ratio	$>4 \times 10^{-2}$	$>3 \times 10^{-6}$
Electron density (cm^{-3})	>33.5	>0.08

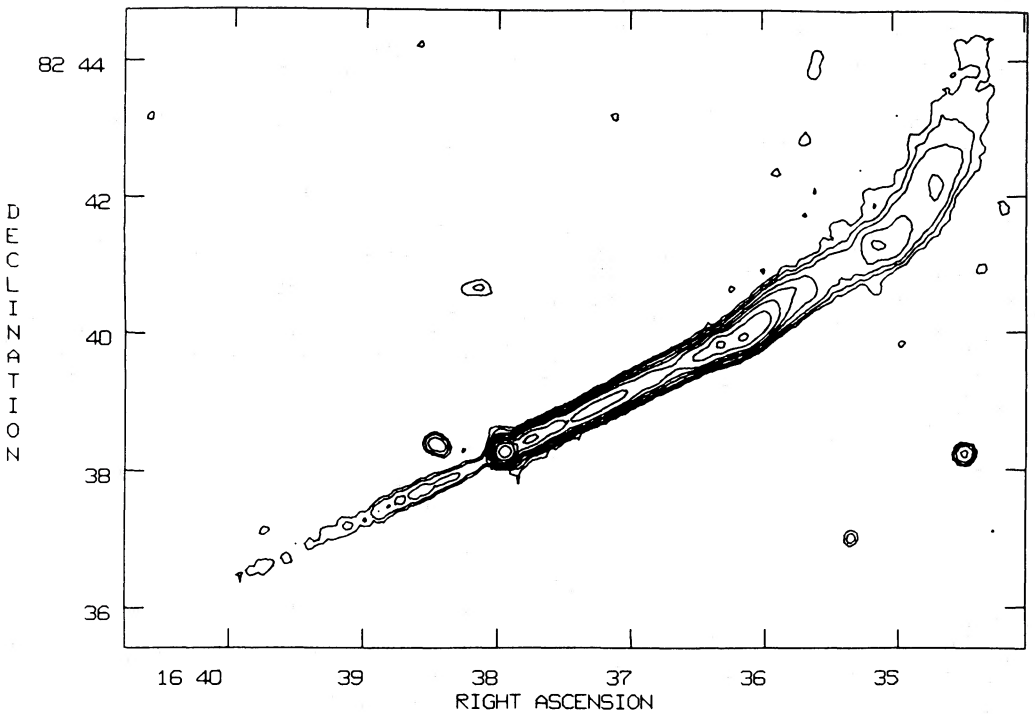

FIG. 10.—Phased array VLA map of NGC 6251 at 18 cm. The contours are −0.03, 0.03, 0.05, 0.1, 0.2, 0.4, 0.8, 1.6, 3.2, 6.4, 12.8, 25, and 50% of the peak, which equals 506 mJy per beam. The 50% contour shows the size of the clean beam (10″).

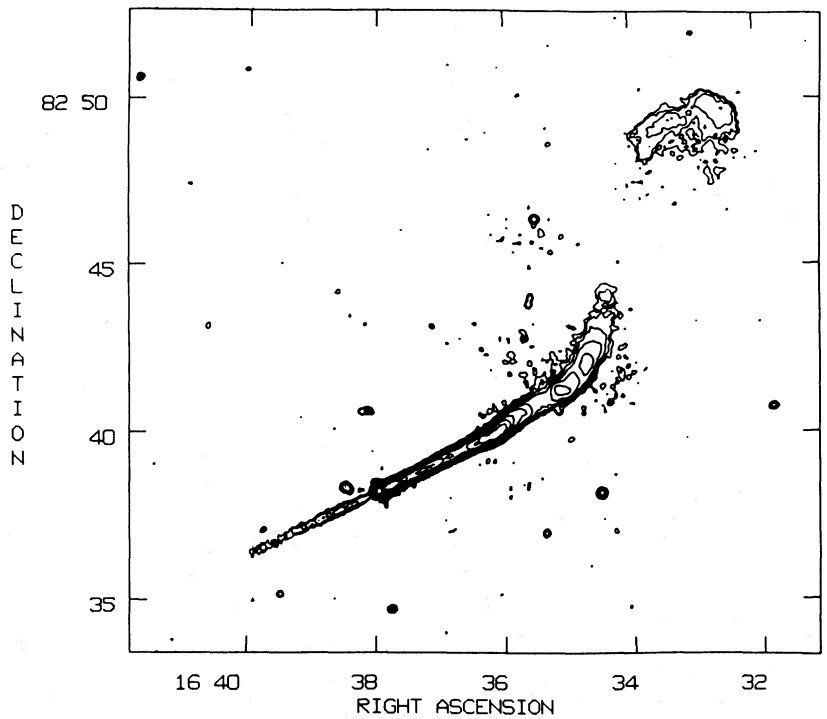

FIG. 11.—Phased array VLA map of NGC 6251 at 18 cm, showing a larger field of view than Fig. 10. The contours are −0.03, 0.03, 0.1, 0.3, 1, 3, 10, 30, and 50% of the peak, which equals 506 mJy per beam. The 50% contour shows the size of the clean beam (10″).

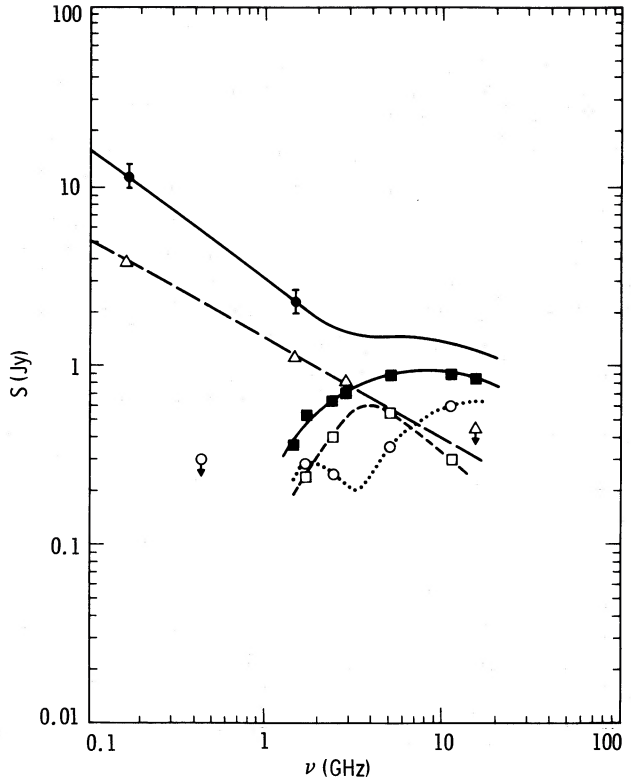

FIG. 12.—Radio spectrum of NGC 6251. *Open circles*, VLBI flux density measurements of the core; *open squares*, VLBI measurements of the flux density of the inner (pc-scale) jet; *filled squares*, total flux density in parsec-scale structure; *open triangles*, measurements of the kiloparsec-scale jet flux densities from Waggett, Werner, and Baldwin (1977); *filled circles*, total flux density measurements from Wagget, Warner, and Baldwin.

The spectral decomposition is based on the measured core and parsec-scale jet flux densities from the available VLBI maps at 18, 13, 6, and 2.8 cm (1.7, 2.3, 5.0, and 10.7 GHz). The values on the upper five lines in Table 3 come from inspection of these spectra and from the VLBI angular size measurements. The core is unresolved on our 18, 13, and 6 cm hybrid maps, and we use an upper limit of 0.2 mas for its size, based on Cohen and Readhead's (1979) 2.8 cm hybrid map. The smaller of the two angular sizes for the inner jet (~ 0.5 mas) is an upper limit to its width at 6 cm. It is not clear what angular size is most appropriate for the jet. The remaining entries in Table 3 are calculated from these measurements. It is not necessary to assume equipartition, since we have information about both radio spectra and angular sizes.

Note that the core and total VLBI flux densities are higher at 18 cm than might have been expected from the other data points, giving the appearance of two separate peaks in the spectrum of the core. This may be partly due to the lower resolution available at the longer wavelength, but it is also possible that the core flux density has increased during the several years between the VLBI experiments at 18 and 13 cm. If this is the case, spectra determined by combining the VLBI measurements from several epochs will be inaccurate. However, there is no evidence for rapid variability of the core of NGC 6251, so we expect that errors introduced by source variability are small. This is supported by the fact that the total core flux density has not changed much over many years, and also by the fact that the two 13 cm VLBI experiments separated by nearly 2 yr showed only small changes in visibility.

The lower limit for the ratio of energy in relativistic particles to energy in magnetic fields decreases by four orders of magnitude from the core to the inner jet. Most of this change is due to a decrease in the lower limits for the particle energy density. If the angular sizes of the core and jet components are near the upper limits listed in Table 3, then both components are magnetic field–dominated rather than particle-dominated. However, if the angular sizes are significantly smaller than these limits, then equipartition or particle dominance could exist, especially in the core.

VI. DEDUCTIONS

a) Is the VLBI Jet Confined?

Can the inner (parsec-scale) jet be pressure-confined? An optically thin sphere of hot gas with a radius of 12 pc will have a thermal bremsstrahlung X-ray luminosity of $\sim 3 \times 10^{32} T_e^{0.5} n_e^2$ ergs s^{-1}, where T_e is the electron temperature and n_e is the electron density (e.g., Morrison 1967; Rybicki and Lightman 1979). The pressure of this gas must be greater than 6×10^{-7} dynes cm^{-2} to confine the inner jet (see § V), giving $n_e T_e > 4 \times 10^9$ cm^{-3} K.

The observed X-ray luminosity of NGC 6251 in the 0.2–3.5 keV band is 1.4×10^{42} ergs s^{-1} (F. Seward, private communication). The total X-ray luminosity of hot gas in the nucleus of NGC 6251 could be higher or lower than this, depending on the spectrum and the angular distribution of the emission. We take the observed value to be an upper limit for the total X-ray luminosity of the nucleus. Hence, $n_e^2 T_e^{0.5} < 5 \times 10^9$.

For temperatures below $\sim 2 \times 10^6$ K, no consistent solution exists, but if we assume an electron temperature of 10^7 K (typical of narrow emission line regions), then the electron density must lie between 400 and 1300 cm^{-3}.

An additional constraint is that this gas must be optically thin at ~ 1 GHz, or we would not see the observed parsec-scale jet at all. This requires the electron density to be less than $\sim 10^4$ cm^{-3} for temperatures $\sim 10^7$ K. This limit does not narrow the allowed range of densities.

Is it plausible that such a large cloud of hot gas exists in the nucleus of NGC 6251? If it is to be gravitationally bound to a central black hole, the mass of the hole must exceed $\sim 10^4 T_e$ solar masses, which is inconsistent with the mass implied by the optical observations of Young *et al.* (1979) for $T_e > \sim 10^6$ K. We therefore conclude that the parsec-scale jet is not pressure-confined. This is consistent with the rapid decrease in brightness seen over the first 12 mas of the NGC 6251 jet, which suggests that the jet may be freely expanding in this region.

A detailed analysis of the collimation properties, equipartition parameters, and X-ray data for the large-scale jet in NGC 6251 led Perley, Bridle, and Willis (1984) to conclude that the first 20″ of the jet are free, while the regions beyond that are confined. Our conclusions here are thus completely compatible with their results.

b) Inverse Compton X-Ray Emission

It is possible, given information about the radio spectrum and angular size of a compact synchrotron radio source, to calculate the X-ray flux density which should be observed from the source due to inverse Compton scattering of radio photons

by the relativistic electrons (Jones, O'Dell, and Stein 1974; Marscher 1983). This is actually a lower limit to the expected X-ray flux density, since other possible mechanisms for producing X-rays are not included. In the case of some "superluminal" radio sources, the predicted X-ray flux density is far greater than the observed level. This discrepancy is used to deduce the existence of bulk relativistic motion in these sources (independent of evidence for relativistic motion from "superluminal" transverse velocities). Can we deduce the existence of bulk relativistic motion in the nucleus of NGC 6251 in the same way?

We assume a simple homogeneous sphere model for the core, and the physical parameter values and spectral decomposition described above. The predicted inverse Compton X-ray flux density from the core component is slightly less than the measured X-ray flux density of ~ 0.3 μJy in the 0.2–3.5 keV band (F. Seward, private communication). Bulk relativistic motion in the core is therefore not required (unless the true size of the core is less than ~ 0.1 mas). A similar calculation of the expected X-ray flux density from the inner jet is more difficult because it is less clear what angular size should be used. Assuming a size greater than 0.5 mas gives a predicted X-ray flux density which is less than the measured value.

VII. THE SMALL- AND LARGE-SCALE ASYMMETRY

There are three simple explanations for the observed asymmetry which should be considered: free-free absorption, intrinsic asymmetry, and relativistic beaming.

a) Free-Free Absorption

One possibility is that the parsec-scale counterjet is hidden by free-free absorption (thermal bremsstrahlung) in a central cloud or disk of dense gas. If this thermal gas is concentrated in a plane which is perpendicular to the radio axis, it will cover the receding jet but not the approaching one. However, this assumes a large covering factor, which is probably unrealistic. The optical depth due to free-free absorption (e.g., Marscher 1979) could be greater than 1 at 1.6 GHz, but this mechanism cannot explain the parsec-scale asymmetry seen at high frequencies (especially 10.7 GHz).

Another major problem with the free-free absorption explanation is that the counterjet would have to be hidden or attenuated much too far from the nucleus for free-free absorption to be plausible, if one wishes to explain the fact that the counterjet is far weaker than the main jet over its entire length. This large-scale difference clearly cannot be due to obscuration by intervening matter. Even if one only wants to explain the parsec-scale asymmetry in this way, the fact that all well-studied radio sources with both large- and small-scale jets have their jets pointing in the same direction tells us that the large- and small-scale asymmetries must be connected in some way. Free-free absorption models cannot explain this connection.

b) Intrinsic Asymmetry

Perhaps the most obvious explanation for the lack of an observed parsec-scale counterjet is that there isn't one. The "central engine" may produce only a one-sided jet, which reverses its direction to produce the two-sided large-scale radio structure (e.g., Rudnick 1982, 1984; Rudnick and Edgar 1984; references in Bridle 1984, p. 140). This idea can be rejected for the same reason as the free-free absorption idea—the evidence that the observed small- and large-scale asymmetries are connected. Thus, if the parsec-scale jet is intrinsically one-sided, we would require that the large-scale jet also be intrinsically one-sided. This gives a switching time of greater than 10^6 yr. But we clearly see a kiloparsec-scale counterjet in NGC 6251, indicating recent energy flow in both directions.

A recent argument in favor of intrinsic large-scale jet asymmetries by Wardle and Potash (1984) is based on the detection of one-sided jets in the eight largest radio sources in a complete sample of 32 quasars from the 4C survey. If the sample sources are really oriented randomly, then these eight objects should lie within 15° of the plane of the sky, and the expected jet/counterjet ratios should be lower than observed. However, the sample is small, and for these calculations care must be taken to exclude emission from the jets, which might be beamed. Furthermore, in a similar sample of 3C quasars (Hough and Readhead 1986), only four of the eight largest sources were found to have one-sided large-scale jets. These two results suggest that there are selection effects in the 3C or 4C samples (or both!) which make it unclear whether the samples are randomly oriented.

A variation of the intrinsic asymmetry models is one in which there are two-sided radio jets, but they appear one-sided due to asymmetric dissipation. That is, the jet on one side is much more efficient at converting beam energy into synchrotron radiation than the jet on the other side. This requires that the same jet remain more (or less) dissipative than the other, all the way from the inner few parsecs out to the extended lobes. The ambient medium through which the jets propagate changes greatly over this large range of scales. Also, the "warm spots" in the extended radio lobes of NGC 6251 are similar in brightness (Willis *et al.* 1982), which implies that approximately equal amounts of energy must be transported to the two lobes on a time scale which is short compared to the radiative lifetimes in the hot spots. This implies that the overall jet efficiencies are not very different. However, the radio emission from the jets may correspond to only a small fraction of the total energy being transported. In this case, the radio brightness of the two jets could be very different even though they transport similar amounts of energy to the lobes.

If this is the explanation for the asymmetric radio structure seen in NGC 6251, then the mechanism responsible for the different radio brightness of the two jets (different shock parameters?) is established within a few parsecs of the core and remains effective for the entire length of the jet. The plausibility of this depends on details of the physical conditions in the jets and the mechanisms which determine the efficiency of radio emission, none of which are well known. Consequently, this explanation cannot be ruled out.

c) Relativistic Beaming

The simplest explanation of both the nuclear and large-scale radio morphology in NGC 6251, and of the fact that in every case thus far the nuclear and large-scale jets point in the same direction, is that the asymmetries are due to relativistic beaming. We assume that the source is composed of two identical, oppositely directed beams with velocity $v = \beta c$ (in the rest frame of the galaxy) and oriented at an angle θ to our line of sight ($\theta \leq 90°$).

A spectral index of -0.5 is typical for the jets in compact radio sources. This is slightly flatter than the spectrum of the kiloparsec-scale jet (for which the spectral index is -0.64; Saunders *et al.* 1981; Bridle and Perley 1983). With a spectral index of -0.5, the jet/counterjet brightness ratio is given by

(Ryle and Longair 1967; Scheuer and Readhead 1979):

$$R = I_{\rm jet}/I_{\rm counterjet} = [(1 + \beta \cos \theta)/(1 - \beta \cos \theta)]^{2.5} .$$

Thus, $\beta \cos \theta = (R^{0.4} - 1)/(R^{0.4} + 1)$.

For the nuclear jet in NGC 6251, we find that $R > 80$. This implies that θ must be less than 45°. If the radio axis of NGC 6251 is really aligned within 45° of our line of sight, then the true linear extent of the well-collimated jet seen in the VLA maps is at least 0.3 Mpc, and the total extent of the source exceeds ~2.5 Mpc.

If relativistic beaming is responsible for the parsec-scale asymmetry, the same mechanism is likely also to be responsible for the large-scale asymmetry, since as mentioned above in all cases known the nuclear and large-scale jets point in the same direction. There have been many estimates of the jet velocity in NGC 6251, but they are all indirect and model-dependent (see Perley, Bridle, and Willis 1984). Consequently, we cannot rule out the possibility of bulk relativistic flow in this jet. It is known that in many radio sources with intermediate-luminosity jets, the counterjets are more than order of magnitude weaker than the main jets (Begelman, Blandford, and Rees 1984). This could be taken as evidence that at least some extended radio jets are relativistically beamed. If this is the case, then the electron density in the jets may be overestimated (Fomalont 1983).

For the strongest double-lobed radio sources, ram pressure confinement of the hot spots requires an expansion velocity of $\sim 0.1c$ (Begelman, Blandford, and Rees 1984), and consequently jet velocities greater than $0.1c$ all the way out to the hot spots. For NGC 6251, we can set a lower limit to $\beta \cos \theta$ by assuming that the kiloparsec-scale jet/counterjet brightness ratio is entirely due to relativistic beaming. This limit is 0.6 for a brightness ratio of greater than 30. If we also assume that the radio axis is oriented at 45° from our line of sight, which is the largest angle consistent with the parsec-scale jet/counterjet brightness ratio, then the bulk velocity of radio-emitting material in the kiloparsec-scale jets is greater than $0.84c$. It is therefore interesting to see whether the large-scale structure can be explained in terms of relativistic jets with bulk velocities of $\sim 0.84c$.

The source exhibits a large-scale S-shaped (inversion) symmetry (e.g., Willis *et al.* 1982). This is the type of symmetry expected if the direction of jet emission has been precessing. However, the apparent precession cone angles are different on the two sides, as are the angular separations between the nucleus and the extended radio lobes, so some mechanism in addition to simple precession is necessary to explain this structure. If the flow velocity in the kiloparsec-scale jets is relativistic, as suggested by the large jet/counterjet brightness ratio, the observed large-scale structure will be distorted by light travel time effects. This will tend to make the counterjet appear more compact, which is not what we observe in this source.

We use the approach of Hjellming and Johnston (1981) and Gower *et al.* (1982) to calculate the appearance of a pair of precessing relativistic jets. If we use a coordinate system in which the plane of the sky is the y-z plane, with the x-axis pointing toward the observer, then the velocity (at time t) of a plasmon which was ejected at time t' is given by

$$v_x = \beta c\{\sin \Psi \sin i \cos [\Phi - \Omega(t - t')] + \cos \Psi \cos i\} ,$$

$$v_y = \beta c \sin \Psi \sin [\Phi - \Omega(t - t')] ,$$

$$v_z = \beta c\{\cos \Psi \sin i - \sin \Psi \cos i \cos [\Phi - \Omega(t - t')]\} ,$$

where βc is the velocity of the plasmon, Ψ is the half-angle of the precession cone, i is the angle between the precession axis and our line of sight (the precession axis is assumed to lie in the x-z plane), Φ is the starting angle for the precession, and Ω is the precession angular velocity. A counterjet would have the opposite sign for all three velocity components. Let D be the distance to the source. Then the apparent angular motion of the plasmon (in radians) is given by

$$\phi_y = v_y(t - t')/\{D[1 - (v_x/c)]\} ,$$

$$\phi_z = v_z(t - t')/\{D[1 - (v_x/c)]\} .$$

To get a snapshot of the appearance of the source, assumed to be composed of many plamons ejected at a steady rate, one can vary t' from t to 0 while holding t fixed.

NGC 6251 is near the eastern edge of the cluster ZwCl 1609.0+8212, and its redshift is within ~100 km s^{-1} of the mean redshift of the cluster members (Sargent, Readhead, and DeBruyn 1986). Thus, it is reasonable to suspect that the large-scale radio structure of NGC 6251 may be affected by a transverse "wind" caused by the motion of the host galaxy through the cluster's intergalactic medium. A good fit to the radio structure on scales larger than ~1 kpc can be obtained with the following model: two identical beams composed of relativistic electrons and positrons precessing about an axis 53° from our line of sight, with bulk velocity $0.84c$. The half-angle of the precession cone is 8°, and the phase is such that the approaching jet makes an angle of 45° to our line of sight at the nucleus. The precession period is $\sim 1.8 \times 10^6$ yr. Both jets have constant opening angles of 3°, and the host galaxy is assumed to be moving to the northwest (position angle 305°) in the plane of the sky with velocity 300 km s^{-1} relative to the local intergalactic medium. The mean electron density of the cluster's intergalactic medium is assumed to be 10^{-5} cm^{-3} (Sargent, Readhead, and DeBruyn 1986).

We assume that the jets are surrounded by a thin "sheath" upon which the intergalactic medium exerts pressure (e.g., Begelman, Rees, and Blandford 1979). Thus, the ram pressure on a given unit length of the jet is determined by the velocity V of the galaxy through the intergalactic medium and the projected cross section of the jet at that point, but not by the flow velocity βc within the jet. We also assume a constant mass per unit length for the jets (no entrainment of material).

The force on a unit length L of the jet due to the pressure of the intergalactic medium (IGM) is $\rho_{\rm IGM} V^2 LD \sin \vartheta$, where $\rho_{\rm IGM}$ is the density of the intergalactic medium, D is the diameter of the jet at the point of interest (obtained from the opening angle), and ϑ is the angle between the local velocity vector of the jet and the direction of the host galaxy's motion through the intergalactic medium (the z-axis). The momentum of a unit length of the jet is $(1 - \beta^2)^{-1/2} \rho_{\rm Jet} \beta c L(\pi/4) D^2$, where the local jet density $\rho_{\rm jet}$ is assumed to be 10^{-3} electrons cm^{-3} at a distance of 100 kpc from the core. Equal numbers of electrons and positrons are also assumed. Over a given time interval (short with respect to the total propagation time of the jet) the force of the IGM "wind" changes the momentum of the jet segment, thus changing its z-velocity and subsequent position. The resulting changes in the jet's appearance over many time intervals were computed numerically. The effect of the "wind" is to contract the linear extent of the main jet and stretch out the counterjet. Figure 13 shows the appearance of the two beams in this model superposed on the WSRT map of Willis *et al.* (1982).

This model can account for the jet/counterjet brightness

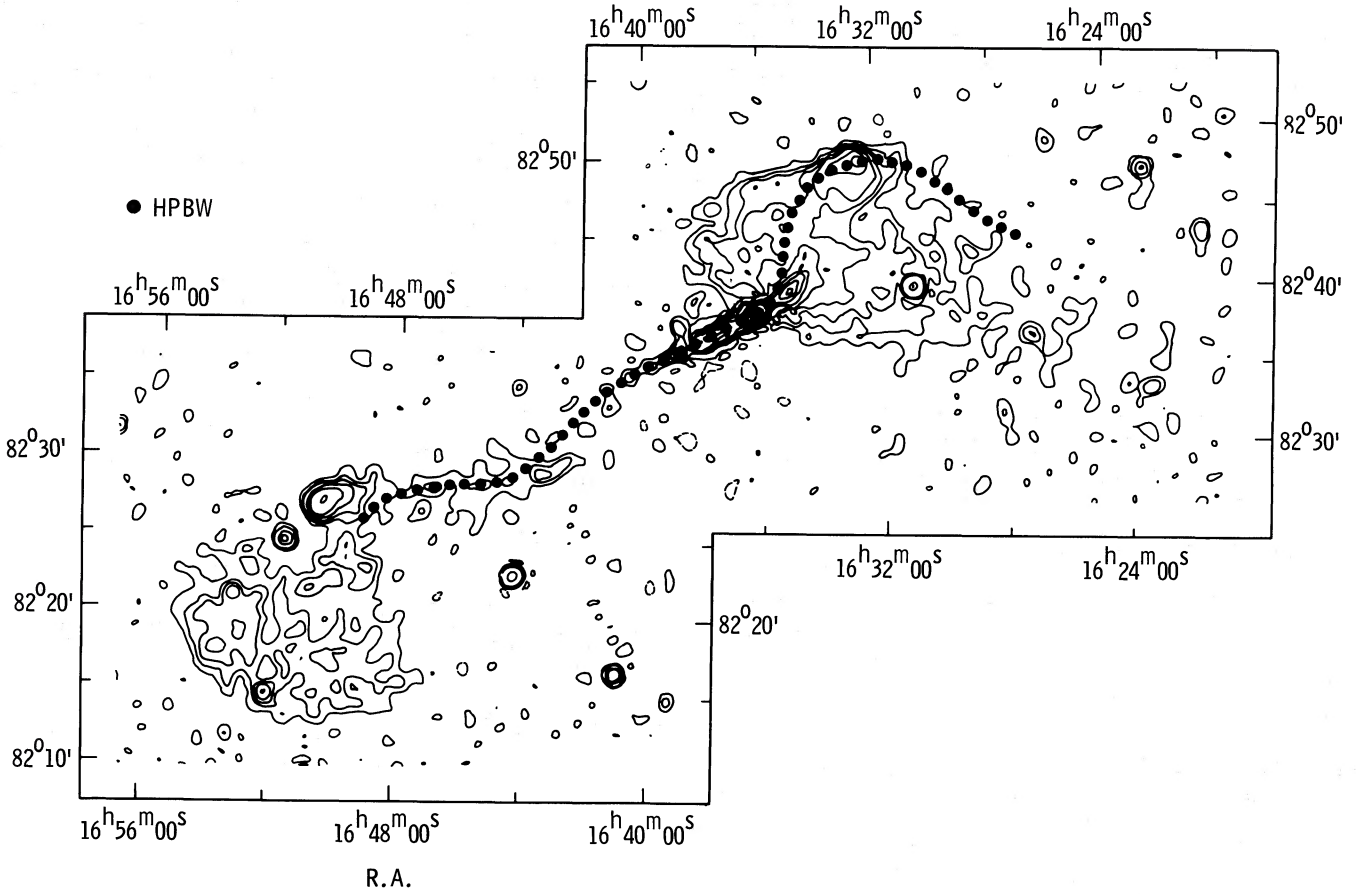

FIG. 13.—Projected appearance of the two beams in the model described in § VII*c* of the text, compared to the WSRT map of Willis *et al.* (1982). The dotted line is the projected appearance of the model.

ratio near the nucleus (30–40 to 1 at a few kpc), as well as the overall shape of the two jet paths. The exact position of the first major bend in the main jet is the least well fit feature of the large-scale structure. The diffuse, low surface brightness emission seen in the WSRT map could be due to the wind sweeping material eastward from the ends of the two beams. In addition, the angle of the jets at the nucleus is just consistent with the limit set by our VLBI observations.

There are two shortcomings to this picture. One is that the jet velocity needs to be very close to c on a parsec scale (it is much more difficult to fit the large-scale structure if the angle of the jets to our line of sight is much less than 45° at the nucleus). Thus, our assumption of constant jet velocities really only applies to regions outside the nucleus. The second problem is that a more massive jet (consisting of electrons and protons instead of electrons and positrons, for example) would require a much higher transverse velocity for the galaxy (>7000 km s^{-1}). Thus, this model requires the jets to transport as little mass as possible. The mass of the jets cannot be dominated by thermal material.

Begelman, Blandford, and Rees (1980) have considered the dynamics of massive black hole binaries. The 1.8×10^6 yr precession period deduced above could be caused by a binary system with the following parameters: mass of the black hole which is responsible for the radio jets of $10^8\ M_\odot$, mass of the other black hole of $10^7\ M_\odot$, and separation of the two black holes of 10^{17} cm. The resulting orbital period is 50 yr, and the radial velocity of the more massive black hole could differ from that of the narrow-line region (assumed to be at rest with respect to the galaxy's center of mass) by as much as 320 km s^{-1}. At this separation, the dynamical evolution time of the binary system is longer than 10^8 yr (Begelman, Blandford, and Rees 1980).

The model described above does not explain details of the observed radio structure in NGC 6251. It is intended only to show that Doppler effects due to bulk relativistic motion on both parsec and kiloparsec scales could be responsible for the general appearance of this source. This does not, of course, prove that the jets in NGC 6251 are in fact relativistic.

VIII. CONCLUSIONS

Our main observational results can be summarized as follows.

1. The jet/counterjet brightness ratio at ± 6 mas from the core of NGC 6251 is at least 80 to 1. This limit is significantly larger than the observed jet/counterjet ratio at $\pm 1'$ from the core.

2. The jet appears to bend through an angle of 3°.5 between about 10 and 25 mas from the core. The total misalignment between the inner jet (at ~ 4 mas) and the kpc jet is 5°.7, and essentially all of this curvature occurs during the first 25 mas of the jet.

3. A knot of increased brightness is seen in the jet at 18 cm at a distance of 25 mas from the core. Future 18 cm VLBI

experiments should attempt to measure the transverse motion of this feature.

4. At 18 cm, the brightness of the radio jet decreases very rapidly during the first 12 mas.

5. The kiloparsec-scale counterjet brightness increases with decreasing distance from the core down to $\sim 1'$, but at smaller distances its brightness decreases.

6. The inner (pc-scale) jet is probably not confined by external hot gas, although the kilo-parsec-scale jet could be.

7. Relativistic beaming could be responsible for the large jet/counterjet brightness ratio on both the small and large scale. If this is so, the radio jet must lie within 45° of our line of sight at the nucleus, and the large-scale radio axis of NGC 6251 is oriented $\sim 53°$ from our line of sight.

8. A measurement of the X-ray flux from NGC 6251 with higher angular resolution might give a much stronger lower limit for the Doppler factor, by showing what fraction of the total X-ray emission is actually coming from the nucleus. This could provide independent evidence for bulk relativistic motion in the central few pc of NGC 6251.

We thank the observatories of the US and European VLBI networks for their contributions to the experiments described here. Astronomical VLBI research at Haystack Observatory, North Liberty Radio Observatory (Iowa), George R. Agassiz Station (Fort Davis), Owens Valley Radio Observatory, and Hat Creek Observatory is supported by the NSF. The National Radio Astronomy Observatory is operated by Associated Universities, Inc., under contract with the NSF. The NASA Deep Space Network is operated by the Jet Propulsion Laboratory, California Institute of Technology, under contract NAS7-100 sponsored by NASA. The Westerbork Synthesis Radio Telescope is operated by the Netherlands Foundation for Radio Astronomy with the support of the Netherlands Organization for the Advancement of Pure Research (ZWO). The Algonquin Radio Observatory and the Dominion Radio Astrophysical Observatory (Penticton) are operated by the National Research Council of Canada. We thank F. Seward of the Harvard-Smithsonian Center for Astrophysics for providing us with *Einstein* IPC data on NGC 6251. In addition, we are grateful for the careful absentee processing of our 18 cm VLBI data by NRAO, and in particular for the valuable help of Bob Vernon.

REFERENCES

Begelman, M. C., Blandford, R. D., and Rees, M. J. 1980, *Nature*, **287**, 307.
———. 1984, *Rev. Mod. Phys.*, **56**, 255.
Begelman, M. C., Rees, M. J., and Blandford, R. D. 1979, *Nature*, **279**, 770.
Bridle, A. H. 1984, in *Proc. NRAO Workshop No. 9, Physics of Energy Transport in Extragalactic Radio Sources*, ed. A. H. Bridle and J. A. Eilek (Green Bank: NRAO), p. 135.
Bridle, A. H., and Perley, R. A. 1983, in *Astrophysical Jets*, ed. A. Ferrari and A. G. Pacholczyk (Dordrecht: Reidel), p. 57.
———. 1984, *Ann. Rev. Astr. Ap.*, **22**, 319.
Burch, S. F. 1977, *M.N.R.A.S.*, **181**, 599.
Clark, B. G. 1973, *Proc. IEEE*, **61**, 1242.
Cohen, M. H., *et al.* 1975, *Ap. J.*, **201**, 249.
Cohen, M. H., and Readhead, A. C. S. 1979, *Ap. J. (Letters)*, **233**, L101.
Cohen, M. H., and Unwin, S. C. 1984, in *IAU Symposium 110, VLBI and Compact Radio Sources*, ed. R. Fanti, K. Kellermann, and G. Setti (Dordrecht: Reidel), p. 95.
Cornwell, T. J. 1981, *VLA Sci. Memo*, No. 135.
Cornell, T. J., and Wilkinson, P. N. 1981, *M.N.R.A.S.*, **196**, 1067.
Fomalont, E. B. 1983, in *Astrophysical Jets*, ed. A. Ferrari and A. G. Pacholczyk (Dordrecht: Reidel), p. 37.
Fomalont, E. B., and Wright, M. C. H. 1974, in *Galactic and Extragalactic Radio Astronomy*, ed. G. L. Verschuur and K. I. Kellermann (New York: Springer), p. 276.
Gower, A. C., Gregory, P. C., Hutchings, J. B., and Unruh, W. G. 1982, *Ap. J.*, **262**, 478.
Hjellming, R. M., and Johnston, K. J. 1981, *Ap. J. (Letters)*, **246**, L141.
Hough, D. H., and Readhead, A. C. S. 1986, in preparation.
Jones, T. W., O'Dell, S. L., and Stein, W. A. 1974, *Ap. J.*, **188**, 353.
Marscher, A. P. 1979, *Ap. J.*, **228**, 27.
———. 1983, *Ap. J.*, **264**, 296.
Miley, G. K. 1980, *Ann. Rev. Astr. Ap.*, **18**, 165.
Moran, J. M. 1976, in *Methods of Experimental Physics*, Vol. **12**, Part C, ed. M. L. Meeks (New York: Academic), p. 174.
Morrison, P. 1967, *Ann. Rev. Astr. Ap.*, **5**, 325.
Perley, R. A., Bridle, A. H., and Willis, A. G. 1984, *Ap. J. Suppl.*, **54**, 291.
Perley, R. A., Willis, A. G., and Scott, J. S. 1979, *Nature*, **281**, 437.
Readhead, A. C. S. 1980, in *IAU Symposium 92, Objects of High Redshifts*, ed. G. O. Abell and P. J. E. Peebles (Dordrecht: Reidel), p. 165.
Readhead, A. C. S., Cohen, M. H., and Blandford, R. D. 1978, *Nature*, **272**, 131.
Rudnick, L. 1982, in *IAU Symposium 97, Extragalactic Radio Sources*, ed. D. S. Heeschen and C. M. Wade (Dordrecht: Reidel), p. 47.
———. 1984, in *Proc. NRAO Workshop No. 9, Physics of Energy Transport in Extragalactic Radio Sources*, ed. A. H. Bridle and J. A. Eilek (Green Bank: NRAO), p. 35.
Rudnick, L., and Edgar, B. K. 1984, *Ap. J.*, **279**, 74.
Rybicki, G. B., and Lightman, A. P. 1979, *Radiation Processes in Astrophysics* (New York: Wiley), p. 162.
Ryle, M., and Longair, M. S. 1967, *M.N.R.A.S.*, **136**, 123.
Sargent, W. L. M., Readhead, A. C. S., and De Bruyn, A. G. 1986, *Pub. A.S.P.*, submitted.
Saunders, R., Baldwin, J. E., Pooley, G. G., and Warner, P. J. 1981, *M.N.R.A.S.*, **197**, 287.
Scheuer, P. A. G., and Readhead, A. C. S. 1979, *Nature*, **277**, 182.
Schwab, F. R., and Cotton, W. D. 1983, *A.J.*, **88**, 688.
Waggett, P. G., Warner, P. J., and Baldwin, J. E. 1977, *M.N.R.A.S.*, **181**, 465.
Wardle, J. F. C., and Potash, R. I. 1984, in *Proc. NRAO Workshop No. 9, Physics of Energy Transport in Extragalactic Radio Sources*, ed. A. H. Bridle and J. A. Eilek (Green Bank: NRAO), p. 30.
Wheeler, J. A. 1971, in *Nuclei of Galaxies*, ed. D. J. K. O'Connell (Pontificiae Academiae Scientiarum Scripta Varia, No. 35; New York: Elsevier), p. 539.
Wilkinson, P. N. 1983, in *Very Long Baseline Interferometry Techniques* (Toulouse: CNES), p. 375.
Willis, A. G., Strom, R. G., Perley, R. A., and Bridle, A. H. 1982, in *IAU Symposium 97, Extragalactic Radio Sources*, ed. D. S. Heeschen and C. M. Wade (Dordrecht: Reidel), p. 141.
Young, P. J., Sargent, W. L. W., Kristian, J., and Westphal, J. A. 1979, *Ap. J.*, **234**, 76.

L. B. BÅÅTH and R. S. BOOTH: Onsala Space Observatory, S-430 00 Onsala, Sweden

J. M. BENSON, A. H. BRIDLE, and J. ROMNEY: NRAO, Edgemont Road, Charlottesville, VA 22903-2475

D. N. FORT: Herzberg Institute of Astrophysics, National Research Council of Canada, Ottawa, Ontario K1A OR6, Canada

J. A. GALT: Dominion Radio Ap. Obs., Box 248, Penticton, B.C. V2A 6K3, Canada

D. L. JONES and R. P. LINFIELD: Mail Code 138-307, Jet Propulsion Laboratory, 4800 Oak Grove Drive, Pasadena, CA 91109

R. L. MUTEL: Physics and Astronomy Department, University of Iowa, Iowa City, IA 52242

I. I. K. PAULINY-TOTH and A. WITZEL: MPI für Radioastronomie, Auf dem Hügel 69, 53 Bonn 1, Federal Republic of Germany

R. A. PERLEY and R. C. WALKER: NRAO, P.O. Box O, Socorro, NM 87801

A. C. S. READHEAD, W. L. W. SARGENT, and S. C. UNWIN: Mail Code 105-24, Caltech, Pasadena, CA 91125

G. A. SEIELSTAD: NRAO, P.O. Box 2, Green Bank, WV 24944

R. S. SIMON: Code 4134S, NRL, Washington, DC 20375

P. N. WILKINSON: University of Manchester, Nuffield Radio Astronomy Labs, Jodrell Bank, Macclesfield, Cheshire SK11 9DL, England